

High-redshift star formation rate up to $z \sim 8.3$ derived from gamma-ray bursts and influence of background cosmology

F. Y. Wang^{*} and Z. G. Dai[†]

Department of Astronomy, Nanjing University, Nanjing 210093, P. R. China

17 November 2018

ABSTRACT

The high-redshift star formation rate (SFR) is difficult to measure directly even by modern approaches. Long-duration gamma-ray bursts (GRBs) can be detected to the edge of the visible universe because of their high luminosities. The collapsar model of long gamma-ray bursts indicates that they may trace the star formation history. So long gamma-ray bursts may be a useful tool of measuring the high-redshift SFR. Observations show that long gamma-ray bursts prefer to form in a low-metallicity environment. We study the high-redshift SFR up to $z \sim 8.3$ considering the *Swift* GRBs tracing the star formation history and the cosmic metallicity evolution in different background cosmological models including Λ CDM, quintessence, quintessence with a time-varying equation of state, and brane-world model. We use latest *Swift* GRBs including two highest- z GRBs, GRB 080913 at $z = 6.7$ and GRB 090423 at $z = 8.3$. We find that the SFR at $z > 4$ shows a steep decay with a slope of ~ -5.0 in Λ CDM. In the other three models, the high-redshift SFR is slightly different from Λ CDM model, and also shows a steep decay.

Key words: Gamma rays: bursts – stars: formation

1 INTRODUCTION

The star formation history (SFH), especially at high-redshift ($z > 6$), is important in many fields in astrophysics. Direct SFR measurements are quite challenging at high-redshift, particularly at the faint end of the galaxy luminosity function. The star formation rate (SFR) has been comprehensively investigated. Hopkins & Beacom (2006) calibrated the star formation history out to $z > 6$ using the ultraviolet and far-infrared data. They found the SFR is tightly constrained at $z < 1$, the SFR in the redshift range of $1 < z < 4$ is approximately a constant and shows a steep decay at $z > 4$ (Hopkins & Beacom 2006). Li (2008) constrained the SFR up to $z = 7.4$ by adding 6 new data and found the same result as Hopkins & Beacom (2006) (Li 2008). The high-redshift SFR can also be determined by observations of color-selected Lyman break galaxies (LBGs) (Bouwens et al. 2008; Mannucci et al. 2007; Verma et al. 2007). Ota et al. (2008) constrained the SFR using Ly α emitters (LAEs) (Ota et al. 2008). In Figure 1, we list the different observational results. We can see that different results disagree with each other even considering the uncertainties.

Long-duration gamma-ray bursts triggered by the death of massive stars, which have been shown to be associated

with supernovae (Stanek et al. 2003; Hjorth et al. 2003), provide a complementary technique for measuring the SFR. GRBs at high redshifts are predicated to be observed because of their high luminosities (Lamb & Reichart 2000; Ciardi & Loeb 2000; Bromm & Loeb 2002, 2006; Gou et al. 2004). The farthest GRB to date is GRB 090423 at $z = 8.3$ (Tanvir et al. 2009; Salvaterra et al. 2009). So GRBs are a promising probe of the star formation history (Totani 1997; Wijers et al. 1998; Porciani & Madau 2001; Bromm & Loeb 2002, 2006; Tutukov 2003). Recent studies show that *Swift* GRBs are not tracing the star formation history exactly but including an additional evolution (Daigne et al. 2006; Cen & Fang 2007; Le & Dermer 2007; Yüksel & Kistler 2007; Salvaterra & Chincarini 2007a; Guetta & Piran 2007; Kistler et al. 2008; Salvaterra et al. 2008; Butler et al. 2009). Observations show that GRBs prefer to form in a low-metallicity environment (Le et al. 2003; Stanek et al. 2006). In the collapsar paradigm, large angular momentum is required to power a GRB. Because high-metallicity stars are expected to have significant mass loss through winds promoting the loss of angular momentum, Langer & Norman (2006) and Woosley & Heger (2006) have argued that GRB progenitors will have a low metallicity (Woosley & Heger 2006; Mészáros 2006; Langer & Norman 2006). This has implications for the expected redshift distribution of GRBs (Natarajan et al. 2005; Salvaterra & Chincarini 2007a; Salvaterra et al. 2007b; Li 2008). Chary et al. (2007) estimated a lower limit

^{*} fayinwang@nju.edu.cn

[†] dzg@nju.edu.cn

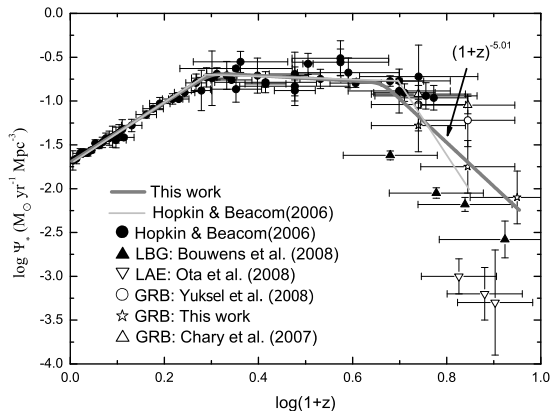


Figure 1. The cosmic star formation history. The black circles are from Hopkins & Beacom (2006). The three open pentagles are the star formation rates at $z = 4.5$, $z = 6$ and $z = 8$ derived using *Swift* GRB data.

of the SFR of 0.12 ± 0.09 and $0.09 \pm 0.05 \text{ M}_{\odot} \text{ yr}^{-1} \text{ Mpc}^{-3}$ at $z = 4.5$ and 6 , respectively, using deep observations of three $z \sim 5$ GRBs with the *Spitzer Space Telescope* (Chary, Berger & Cowie 2007). Yüksel et al. (2008) used *Swift* GRB data to constrain the high-redshift SFR and found that no steep drop exists in the SFR up to $z \sim 6.5$ (Yüksel et al. 2008). Kistler et al. (2009) constrained SFR up to $z \sim 8$ using four-years *Swift* data and found SFR to beyond $z = 8$ was consistent with LBG-based measurements (Kistler et al. 2009).

In this paper, we estimate the high-redshift SFR using latest *Swift* long-duration GRBs, considering the GRB formation rate tracing SFH and the cosmic metallicity evolution. We use the SFR between $z = 1$ and $z = 4$ and relate the GRB counts in this redshift bin. The absolute conversion factor between the SFR and the GRB rate is highly uncertain. But we do not need this factor in this method. Because weak low-redshift GRBs can not be seen at high redshifts, so we only use high luminosity GRBs. We proceed analogously to Yüksel et al. (2008). But there are two differences between our method and Yüksel's method. First, we consider that long GRBs prefer to form in low-metallicity regions and trace the star formation history, but Yüksel et al. (2008) and Kistler et al. (2009) considered GRBs do not trace star formation history directly, instead implying some kind of additional evolution. Second, we examine the influence of background cosmology. In 1998, observations on type Ia supernovae suggest the accelerating universe. Many models have been proposed to explain the accelerating expansion. Out of many particular models, we focus on four representative models: Λ CDM, quintessence, quintessence with time-varying equation of state, and brane-world.

The structure of this paper is as follows. In section 2, we introduce the method. In section 3, we show our results on high-redshift SFR. Finally, section 4 contains conclusions and discussions.

2 THE METHOD

More recent observational studies indicated that the long GRB host galaxy metallicity is generally lower than that of the average massive star forming galaxies (Le et al. 2003; Stanek et al. 2006). Salvaterra & Chincarini (2007) found that the differential peak flux number counts obtained by BATSE and *Swift* could be well fitted using GRBs forming in low-metallicity galaxies (Salvaterra & Chincarini 2007a). Under the assumption that the formation of GRBs follows the cosmic star formation history and GRBs form preferentially in low-metallicity galaxies, the GRB formation rate is given by

$$\Psi_{\text{GRB}}(z) = k_{\text{GRB}} \Sigma(Z_{\text{th}}, z) \Psi_*(z), \quad (1)$$

where k_{GRB} is the GRB formation efficiency, $\Sigma(Z_{\text{th}}, z)$ is the fraction of galaxies at redshift z with metallicity below Z_{th} (Langer & Norman 2006) and $\Psi_*(z)$ is the observed comoving SFR. The redshift distribution of observable GRBs is

$$\frac{dN}{dz} = F(z) / \langle f_{\text{beam}} \rangle \Sigma(Z_{\text{th}}, z) \Psi_*(z) \frac{dV/dz}{1+z}, \quad (2)$$

where $F(z)$ represents the ability both to detect the trigger of burst and to obtain the redshift (Kistler et al. 2008). The redshifts of high-redshift GRBs are determined by a spectral break in near infrared or infrared bands. Many ground-based facilities could recognize the spectral break and then obtain the redshift. GROND observed the spectral break of GRB080913 between i' and z' bands and the redshift of GRB080913 is $z=6.7$ (Greiner et al. 2009). Greiner et al. (2009) show that 2m-class telescopes can identify most high-redshift GRBs. The redshift of GRB090423 is determined by NIR spectroscopic observations (Tanvir et al. 2009; Salvaterra et al. 2009). So if the luminosities of high-redshift GRBs are high enough and spacecrafts (such as *Swift* and *Fermi*) can detect, the redshifts can be obtained using ground-based facilities. $\langle f_{\text{beam}} \rangle$ is the beaming factor and dV/dz is the comoving volume element per unit redshift, given by

$$\frac{dV}{dz} = \frac{4\pi c d_L^2 H(z)}{1+z} \quad (3)$$

The luminosity distance, d_L , to a source at redshift z is

$$d_L = c(1+z) \int_0^z \frac{1}{H(z')} dz', \quad (4)$$

with

$$H(z) = H_0 \sqrt{\Omega_m (1+z)^3 + \Omega_\Lambda} \quad (5)$$

in a flat Λ CDM universe. For bursts with luminosities sufficient to be viewed within an entire redshift range, Kistler et al. (2008) found that $F(z)$ could be set to a constant (for more details, see Kistler et al. 2008, 2009).

Some theoretical models (Woosley & Heger 2006; see Mészáros 2006 for a review) require that GRB progenitors should have metallicity $\leq 0.1 Z_{\odot}$. According to Langer & Norman (2006), the fractional mass density belonging to metallicity below a given threshold Z_{th} is (Langer & Norman 2006)

$$\Sigma(Z_{\text{th}}, z) = \frac{\hat{\Gamma}[\alpha_1 + 2, (Z_{\text{th}}/Z_{\odot})^2 10^{0.15\beta z}]}{\Gamma(\alpha_1 + 2)}, \quad (6)$$

where $\hat{\Gamma}$ and Γ are the incomplete and complete gamma functions, $\alpha_1 = -1.16$ is the power-law index in the Schechter distribution function of galaxy stellar masses (Panter, Heavens & Jimenez 2004) and $\beta = 2$ is the slope of the galaxy stellar mass-metallicity relation (Savaglio et al. 2005; Langer & Norman 2006). We adopt $Z_{\text{th}} = 0.1Z_{\odot}$ as in Langer & Norman (2006).

We show the luminosity-redshift distribution of 119 long GRBs observed by *Swift*¹ till GRB 090529 in Figure 2. The isotropic luminosity is

$$L_{\text{iso}} = E_{\text{iso}}/[T_{90}/(1+z)], \quad (7)$$

where E_{iso} is the isotropic energy in the $1-10^4$ keV band and T_{90} is the GRB duration. Because only bright bursts can be seen at low and high redshifts, so we choose the luminosity cut $L_{\text{iso}} > 3 \times 10^{51}$ ergs s^{-1} (Yüksel et al. 2008). There are four groups of GRBs defined by this L_{iso} cut in $z = 1-4$, $4-5$, $5-7$, and $7-8.5$. The GRBs in $z = 1-4$ act as a “control group” to base the GRB to SFR conversion, since this redshift bin has both good SFR measurements and GRB counts. We calculate the theoretically predicated number of GRBs in this bin as

$$\begin{aligned} N_{1-4}^{\text{the}} &= \Delta t \frac{\Delta\Omega}{4\pi} \int_1^4 dz F(z) \Sigma(Z_{\text{th}}, z) \frac{\Psi_*(z)}{\langle f_{\text{beam}} \rangle} \frac{dV/dz}{1+z} \\ &= A \int_1^4 dz \Sigma(Z_{\text{th}}, z) \Psi_*(z) \frac{dV/dz}{1+z}, \end{aligned} \quad (8)$$

where $A = \Delta t \Delta\Omega F_0/4\pi \langle f_{\text{beam}} \rangle$ depends on the total time, Δt , and the angular sky coverage, $\Delta\Omega$. The theoretical number in $z = 4-5$ and $5-7$ can be written by

$$N_{z_1-z_2}^{\text{the}} = \langle \Psi_* \rangle_{z_1-z_2} A \int_{z_1}^{z_2} dz \Sigma(Z_{\text{th}}, z) \frac{dV/dz}{1+z}, \quad (9)$$

where $\langle \dot{\rho}_* \rangle_{z_1-z_2}$ is the average SFR density in the redshift range z_1-z_2 . Representing the predicated numbers, $N_{z_1-z_2}^{\text{the}}$ with the observed GRB counts, $N_{z_1-z_2}^{\text{obs}}$, we obtain the SFR in the redshift range z_1-z_2

$$\langle \Psi_* \rangle_{z_1-z_2} = \frac{N_{z_1-z_2}^{\text{obs}} \int_1^4 dz \frac{dV/dz}{1+z} \Sigma(Z_{\text{th}}, z) \Psi_*(z)}{N_{1-4}^{\text{obs}} \int_{z_1}^{z_2} dz \frac{dV/dz}{1+z} \Sigma(Z_{\text{th}}, z)}. \quad (10)$$

Below, we briefly introduce three other cosmological models in which we calculate the high-redshift SFR. We will restrict our attention to flat models ($k = 0$) because the flat geometry is strongly supported by five-years WMAP data (Komatsu et al. 2009).

We first consider the dark energy with a constant equation of state $w(z) = w_0$, where $-1 < w < -1/3$. In such a case this component is called “quintessence”. Confrontation with recent observational datasets, Wang et al. (2007) found $\Omega_M = 0.31$ and $w_0 = -0.95$. We use these data in the following calculations (Wang, Dai & Zhu 2007). The luminosity-redshift distribution of GRBs in this model is shown in Figure 3.

If we consider that the quintessence arises from an evolving scalar field, it would be natural to expect that the equation of state should vary with time. We consider $w(z) = w_0 + w_1 z/(1+z)$. We also use the results of Wang et al. (2007), $\Omega_M = 0.30$, $w_0 = -1.08$ and $w_1 = 0.84$ (Wang,

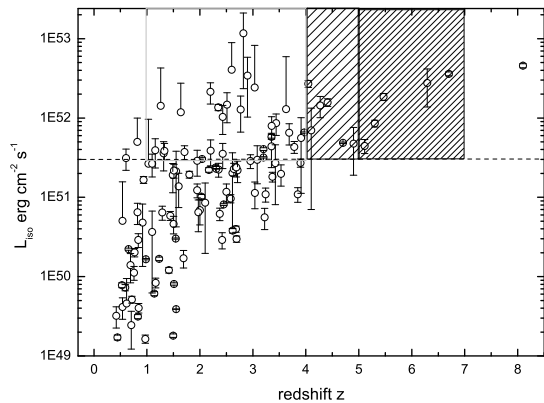


Figure 2. The luminosity-redshift distribution of 119 *Swift* long duration GRBs in the Λ CDM model. The number counts in redshift bins $z = 1-4$, $4-5$, $5-7$, and $7-8.5$ are 28, 6, 5, and 1 respectively.

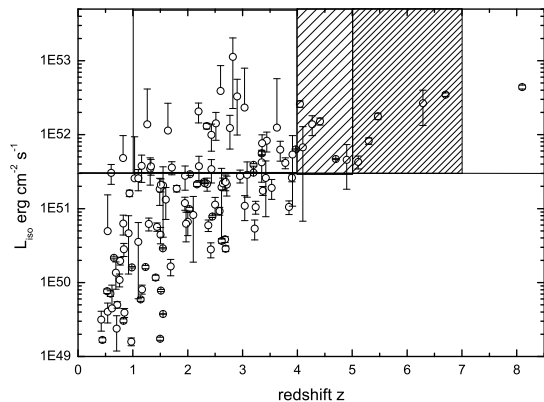


Figure 3. The luminosity-redshift distribution of 119 *Swift* long duration GRBs in the quintessence ($w = w_0$) model. The number counts in redshift bins $z = 1-4$, $4-5$, $5-7$, and $7-8.5$ are 27, 6, 5, and 1 respectively.

Dai & Zhu 2007). The luminosity-redshift distribution of GRBs in this model is shown in Figure 4.

Brane-world scenarios assume that our four-dimensional space-time is embedded into five-dimensional space (Deffayet, Davli & Gabadadze 2002). Gravity in five dimensions is governed by the usual five-dimensional Einstein-Hilbert action. The bulk metric induces a four-dimensional metric on the brane. We consider the flat Dvali-Gabadadze-Porrati model. The only parameter is Ω_M . We use the result from Wang et al. (2009), $\Omega_M = 0.20$ (Wang, Dai & Qi 2009). The luminosity-redshift distribution of GRBs in this model is shown in Figure 5.

The SFR conversion from one cosmology to another is as follows. In the flat universe, the comoving volume is proportional to comoving distance cubed, $V_c \propto D_c^3$, and the comoving volume between redshifts $z - \Delta z$ and $z + \Delta z$ is

¹ See http://swift.gsfc.nasa.gov/docs/swift/archive/grb_table.

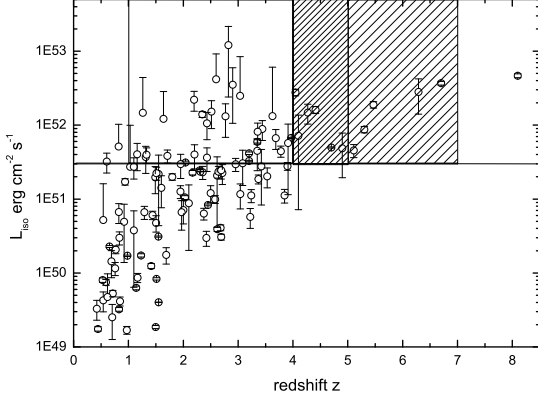


Figure 4. The luminosity-redshift distribution of 119 *Swift* long duration GRBs in the quintessence with a time-varying equation of state ($w = w_0 + w_1 z / (1 + z)$). The number counts in redshift bins $z = 1 - 4$, $4 - 5$, $5 - 7$, and $7 - 8.5$ are 30, 6, 5, and 1 respectively.

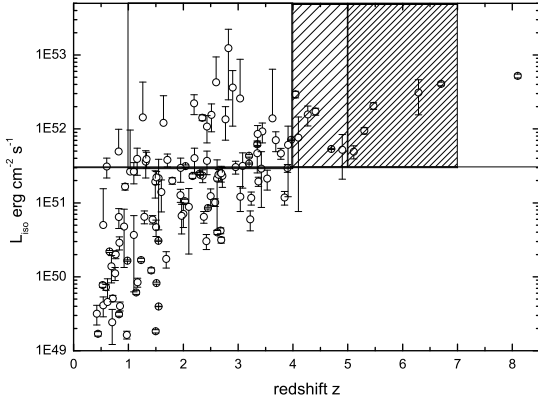


Figure 5. The luminosity-redshift distribution of 119 *Swift* long duration GRBs in the brane-world model. The number counts in redshift bins $z = 1 - 4$, $4 - 5$, $5 - 7$, and $7 - 8.5$ are 31, 6, 5, and 1 respectively.

$V_c(z, \Delta z) \propto D_c^3(z + \Delta z) - D_c^3(z - \Delta z)$. Since the luminosity is proportional to the comoving distance squared, $L \propto D_c^2$, the SFR density for a given redshift range is (Hopkins 2004)

$$\Psi_*(z) \propto \frac{L(z)}{V_c(z, \Delta z)} \propto \frac{D_c^2(z)}{D_c^3(z + \Delta z) - D_c^3(z - \Delta z)}. \quad (11)$$

The Hubble functions in different dark energy models are showed in Table 1. We convert the SFR in the redshift range $z = 1 - 4$ in Λ CDM to other models. The derived SFR can be used to calculate the high-redshift SFR in quintessence, quintessence with a time-varying equation of state and brane-world model.

Table 2. The high-redshift SFRs in four models.

Model	Redshift	Star formation rate
Λ CDM	4.5 ± 0.5	$\text{Log}\Psi_* = -1.287 \pm 0.30$
Λ CDM	6.0 ± 1.0	$\text{Log}\Psi_* = -1.750 \pm 0.30$
Λ CDM	8.0 ± 0.5	$\text{Log}\Psi_* = -2.110 \pm 0.30$
Quintessence	4.5 ± 0.5	$\text{Log}\Psi_* = -1.296 \pm 0.30$
Quintessence	6.0 ± 1.0	$\text{Log}\Psi_* = -1.787 \pm 0.30$
Quintessence	8.0 ± 0.5	$\text{Log}\Psi_* = -2.287 \pm 0.30$
Var Quintessence	4.5 ± 0.5	$\text{Log}\Psi_* = -1.394 \pm 0.30$
Var Quintessence	6.0 ± 1.0	$\text{Log}\Psi_* = -1.819 \pm 0.30$
Var Quintessence	8.0 ± 0.5	$\text{Log}\Psi_* = -2.214 \pm 0.30$
Brane-world	4.5 ± 0.5	$\text{Log}\Psi_* = -1.466 \pm 0.30$
Brane-world	6.0 ± 1.0	$\text{Log}\Psi_* = -1.905 \pm 0.30$
Brane-world	8.0 ± 0.5	$\text{Log}\Psi_* = -2.205 \pm 0.30$

3 THE DERIVED HIGH-REDSHIFT STAR FORMATION RATE

In Figure 1, we show the measurement of the high-redshift SFR in the Λ CDM model with $\Omega_M = 0.27$, $\Omega_\Lambda = 0.73$ and $H_0 = 70 \text{ km s}^{-1} \text{ Mpc}^{-1}$. The star formation rates are $\text{Log}\Psi_* = -1.287 \pm 0.30$, $\text{Log}\Psi_* = -1.750 \pm 0.30$, and $\text{Log}\Psi_* = -2.110 \pm 0.30 \text{ M}_\odot \text{ yr}^{-1} \text{ Mpc}^{-3}$ at $z = 4.5$, 6.0 , and 8.0 , respectively. Taking into account the Poisson confidence interval for four observed GRBs, we assign a statistical uncertainty of a factor of 2 (Yüksel et al. 2008). The derived high-redshift SFR shows a steep decay with a slope of about 5.0 (the slope of Hopkins & Beacom (2006) is about 7.8). If we exclude a particular GRB or changes in redshift ranges, the derived SFR will change insignificantly. This conclusion is consistent with Yüksel et al. (2008), but the derived high-redshift SFR is different from that of Yüksel et al. (2008). The main reason is that we consider GRBs prefer to form in low-metallicity regions.

We show the update SFH fit of Hopkins & Beacom (2006) at high-redshifts based on our new GRB results. We use a continuous form of a broken power law (Yüksel et al. 2008),

$$\Psi_*(z) = \Psi_{*,0} \left\{ [(1+z)^a]^\eta + \left[\frac{(1+z)^b}{(1+z_1)^{b-a}} \right]^\eta + \left[\frac{(1+z)^c}{(1+z_1)^{b-a}(1+z_2)^{c-b}} \right]^\eta \right\}^{1/\eta}, \quad (12)$$

where using $\eta \simeq -10$ smoothes the power law transitions. Our fitted result is shown by the thick gray line in Fig 1. Here, $z_1 = 1$ and $z_2 = 4.0$ are the redshifts of the breaks, $a = 3.4$, $b = -0.3$ and $c = -5.0$ is the slopes of these three power laws, and the normalization is $\Psi_{*,0} = 0.02 \text{ M}_\odot \text{ yr}^{-1} \text{ Mpc}^{-3}$.

In Table 2, we show the high-redshift SFRs in four cosmological models. The value of SFR in these models show no remarkable difference. The reasons are as follows. First, the GRB counts in redshift bins are different because the luminosity distances in these models are not equal. Second, the comoving volume of these models are different. Third, there is a conversion factor from one cosmological model to another. The derived SFR in these cosmological models are consistent with each other in quoted uncertainties. The influence of background cosmology can be neglected when we use this method to measure the high-redshift SFR.

Table 1. Expansion rates $H(z)$ in four models. We consider the flat universe. In the brane-world model, $\Omega_{rc} = (1 - \Omega_m^2)/4$.

Model	Cosmological expansion rate $H(z)$.
Λ CDM	$H^2(z) = H_0^2 [\Omega_m (1+z)^3 + 1 - \Omega_m]$
Quintessence	$H^2(z) = H_0^2 [\Omega_m (1+z)^3 + (1 - \Omega_m) (1+z)^{3(1+w)}]$
Var Quintessence	$H^2(z) = H_0^2 [\Omega_m (1+z)^3 + (1 - \Omega_m) (1+z)^{3(1+w_0-w_1)} \exp(3w_1z)]$
Braneworld	$H^2(z) = H_0^2 \left[(\sqrt{\Omega_m(1+z)^3 + \Omega_{rc}} + \sqrt{\Omega_{rc}})^2 \right]$

4 CONCLUSIONS AND DISCUSSIONS

In this paper, we constrain the high-redshift SFR up to $z \sim 8.3$ using the latest *Swift* GRB data including two highest- z GRBs, GRB 080913 at $z = 6.7$ and GRB 090423 at $z = 8.3$ in four background cosmological models. We consider that GRBs trace the star formation history and prefer to form in a low-metallicity environment. The empirical method is similar to Yüksel et al. (2008) and Kistler et al. (2009). This method has two advantages. First, statistics of the recent *Swift* GRB data allowed the use of luminosity cuts to fairly compare GRBs in the full redshift range, eliminating the unknown GRB luminosity function. Second, we can calculate the high-redshift SFR by comparing the counts of GRBs at different redshift ranges, normalized to SFR data at intermediate redshifts which have been well constrained by observations, eliminating the need for knowledge of the GRB efficiency factor. But there are two differences between our method and Yüksel's method. First, we consider that long GRBs prefer to form in low-metallicity regions and trace the star formation history, but Yüksel et al. (2008) and Kistler et al. (2009) considered GRBs do not trace star formation history directly, instead implying some kind of additional evolution. Second, we examine the influence of background cosmology.

Our results show that the SFR at $z > 4$ shows a steep decay with a slope of about -5.0 in Λ CDM. In three other models, the high-redshift SFR is slightly different from that in the Λ CDM model, and also shows a steep decay. Yüksel et al. (2008) found the decay slope was -3.5 at $z > 4$. Our derived high-redshift SFR is different from Yüksel et al. (2008). The main reason is that we consider GRBs prefer to form in low-metallicity regions. Li (2008) derived the SFH up to $z = 7.4$, and found that the decay slope at $z > 4$ was 4.48 (Li 2008). Their result is consistent with ours.

ACKNOWLEDGMENTS

We thank A. M. Hopkins and H. Yüksel for sharing the SFR data. This work was supported by the National Natural Science Foundation of China (grants 10233010, 10221001 and 10873009) and the National Basic Research Program of China (973 program) No. 2007CB815404. F. Y. Wang was also supported by Jiangsu Project Innovation for PhD Candidates (CX07B-039z).

REFERENCES

- Bouwens, R. J., et al. 2008, ApJ, 686, 230
 Bromm, V., & Loeb, A. 2002, ApJ, 575, 111
 Bromm, V., & Loeb, A. 2006, ApJ, 642, 382
 Butler, N. R., Bloom, J. S. & Poznanski, D., 2009, arXiv:0910.3341
 Cen, R. & Fang, T., 2007, arXiv: 0710.4370
 Chary, R., Berger, E., & Cowie, L. 2007, ApJ, 671, 272
 Ciardi, B., & Loeb, A. 2000, ApJ, 540, 687
 Daigne, F., Rossi, E. M. & Mochkovitch, R., 2006, MNRAS, 372, 1034
 Deffayet, C., Dvali, G. & Gabadadze, G. 2002, Phys. Rev. D, 65, 044023
 Gou, L. J. et al. 2004, ApJ, 604, 508
 Guetta, D., & Piran, T. 2007, J. Cosmol. Astropart. Phys., 7, 3
 Hjorth, J., et al. 2003, Nature, 423, 847
 Hopkins, A. M. 2004, ApJ, 615, 209
 Hopkins, A. M., & Beacom, J. F. 2006, ApJ, 651, 142
 Kistler, M. D., et al. 2008, ApJ, 673, L119
 Kistler, M. D., et al. 2009, arXiv:0906.0590
 Komatsu, E. et al. 2009, ApJS, 180, 283
 Lamb, D. Q., & Reichart, D. E. 2000, ApJ, 536, 1
 Langer, L., & Norman, C. A. 2006, ApJ, 638, L63
 Le Floc'h et al. 2003, A&A, 400, 499
 Le, T., & Dermer, C. D. 2007, ApJ, 661, 394
 Li, L. X. 2008, MNRAS, 388, 1487
 Mannucci, F., et al. 2007, A&A, 461, 423
 Mészáros, P. 2006, Rep. Prog. Phys, 69, 2259
 Natarajan, P., et al. 2005, MNRAS, 364, L8
 Ota, K., et al. 2008, ApJ, 677, 12
 Panter, B., Heavens, A. F., & Jimenez, R. 2004, MNRAS, 355, 764
 Porciani, C. & Madau, P. 2001, ApJ, 548, 522
 Salvaterra, R., & Chincarini, G. 2007a, ApJ, 656, L49
 Salvaterra, R., et al. 2007b, MNRAS, 380, L45
 Salvaterra, R., et al. 2008, arXiv:0805.4104
 Salvaterra, R., et al. 2009, arXiv:0906.1578
 Savaglio, S., et al. 2005, ApJ, 635, 260
 Stanek, K. Z., et al. 2003, ApJ, 591, L17
 Stanek, et al. 2006, Acta Astronomica, 56, 333
 Tanvir, N. R. et al. 2009, arXiv:0906.1577
 Totani, T. 1997, ApJ, 486, L71
 Tutukov, A. V. 2003, Astron. Rep. 47,637
 Verma, A., et al. 2007, MNRAS, 377, 1024
 Wang, F. Y., Dai, Z. G. & Zhu, Z. H., 2007, ApJ, 667, 1
 Wang, F. Y., Dai, Z. G. & Qi, S., 2009, A&A, 507, 53
 Wijers, R. A. M. J. et al. 1998, MNRAS, 294, L13

Woosley, S. E. & Heger, A. 2006, 637, 914

Yüksel, H., & Kistler, M. D. 2007, Phys. Rev. D, 75, 083004

Yüksel, H., et al. 2008, ApJ, 683, L5